Available online at www.sciencedirect.com
ScienceDirect
C. R. Chimie 10 (2007) 721–730
COMPTES RENDUS CHIMIE
http://france.elsevier.com/direct/CRAS2C/

Full paper / Mémoire

Iridium aminyl radical complexes as catalysts for the catalytic dehydrogenation of primary hydroxyl functions in natural products

Nicola Donati [a], Martin Königsmann [a], Daniel Stein [a], Lyn Udino [b], Hansjörg Grützmacher [a,*]

[a] *Department of Chemistry and Applied Biosciences, ETH Hönggerberg, Campus Fouillole, 97159, CH-8093 Zürich, Switzerland*
[b] *Département de chimie, Université des Antilles et de la Guyane, BP 250, 97157 Pointe-à-Pitre cedex, Guadeloupe*

Received 24 January 2007; accepted after revision 26 March 2007
Available online 15 May 2007

Abstract

The cationic tetra-coordinated 16 electron complex $[Ir(trop_2dach)]^+OTf^-$ (**1**) where ($OTf^- = CF_3SO_3^-$) and the neutral amine amido complex [Ir(trop$_2$dach-1H)] (**2**) were isolated and structurally characterized. The NH function in **1** is easily deprotonated ($pK_a^{DMSO} = 10.5$) to yield the amino amido complex [Ir(trop$_2$dach-1H)] (**2**), which is deprotonated at $pK_a^{DMSO} = 19.6$ to the anionic di(amido) iridate $[Ir(trop_2dach\text{-}2H)]^-$ (**3**); [(*R*,*R*)-trop$_2$dach stands for the tetrachelating diamino diolefin ligand (*R*,*R*)-*N*,*N*′-bis(5*H*-dibenzo[*a*,*d*]cyclohepten-5-yl)-1,2-diaminocyclohexane; (*R*,*R*)-trop$_2$dach-1H and (*R*,*R*)-trop$_2$dach-2H indicate the mono and double deprotonated form]. Complex **3** is easily oxidized by 1,4-benzoquinone (**BQ**) to the neutral iridium aminyl radical complex $[Ir(trop_2dach\text{-}2H)]^\bullet$ (**4**). In combination with **BQ** as hydrogen acceptor and catalytic amounts of base, **4** serves as catalyst in the highly efficient dehydrogenation of functionalized primary alcohols to the corresponding aldehydes, $RCH_2OH + \mathbf{BQ} \rightarrow RCH{=}O + \mathbf{H_2BQ}$ ($\mathbf{H_2BQ}$ = catechol). Alcohols like geraniol and retinol are rapidly converted to geranial and retinal, while the conversion of sterically hindered alcohols like lavandulol is slower and the primary product, lavandulal, isomerizes to isolavandulal in a classical base-catalyzed reaction. ***To cite this article: N. Donati et al., C. R. Chimie 10 (2007).***

Résumé

Le complexe cationique tétracoordiné $[Ir(trop_2dach)]^+OTf^-$ (**1**) et le complexe neutre amine amido [Ir(trop$_2$dach-1H)] (**2**) ont été isolés, et leur caractérisation structurale effectuée ($OTf^- = CF_3SO_3^-$). La déprotonation aisée de **1** ($pK_a^{DMSO} = 10.5$) conduit au complexe amino amido [Ir(trop$_2$dach-1H)] (**2**), dont la déprotonation à $pK_a^{DMSO} = 19.6$ conduit au di(amido) iridate anionique $[Ir(trop_2dach\text{-}2H)]^-$ (**3**); [(*R*,*R*)-trop$_2$dach représente le ligand tétradenté diamino diolefine (*R*,*R*)-*N*,*N*′-bis(5*H*-dibenzo[*a*,*d*]cyclohepten-5-yl)-1,2-diaminocyclohexane ; (*R*,*R*)-trop$_2$dach-1H and (*R*,*R*)-trop$_2$dach-2H indiquent respectivement les formes déprotonées une fois et deux fois]. L'oxydation aisée du complexe **3** par la 1,4-benzoquinone (**BQ**) conduit au complexe radicalaire aminyl iridium neutre $[Ir(trop_2dach\text{-}2H)]^\bullet$ (**4**). En présence d'une quantité catalytique de base et combiné à **BQ** (acepteur d'hydrogène) **4** est un excellent catalyseur dans la réaction d'oxydation d'alcools primaires, conduisant aux aldéhydes correspondants,

* Corresponding author.
E-mail address: gruetzmacher@inorg.chem.ethz.ch (H. Grützmacher).

1631-0748/$ - see front matter © 2007 Académie des sciences. Published by Elsevier Masson SAS. All rights reserved.
doi:10.1016/j.crci.2007.03.017

$RCH_2OH + \mathbf{BQ} \rightarrow RCH{=}O + \mathbf{H_2BQ}$ ($\mathbf{H_2BQ}$ = catéchol). Des alcools naturels tels le géraniol et le rétinol sont rapidement oxydés en géranial et rétinal. Cependant, l'oxydation des alcools où il existe un encombrement stérique, tel le lavandulol, est plus lente. Le lavandulal obtenu s'isomérise en isolavandulal au cours d'une réaction classique catalysée en milieu basique. ***Pour citer cet article : N. Donati et al., C. R. Chimie 10 (2007).***

Keywords: Aminyl radicals; Alcohols; Aldehydes; Catalysis; Iridium; Natural products; Oxidation

Mots-clés : Alcohols ; Aldehydes ; Catalyse ; Iridium ; Oxydation ; Produits naturelles ; Radicale aminyle

1. Introduction

Galactose oxidase (GOase) is a copper-dependent metalloenzyme which converts primary hydroxyl functions into aldehydes with high turn-over frequencies of about 800 s^{-1} (2.8×10^6 h^{-1}) [1]. The enzyme is very selective and secondary hydroxyl groups are not converted. A wide range of different primary alcohols can be employed as substrates. Extensive investigations with the enzyme and model complexes [2–8] allowed obtaining a rather precise picture of the mechanism. In simplified form this consists in: (*i*) substrate (=alkoxide) binding to a Cu(II) tyrosinyl radical complex to give a [Cu(II)($^{\bullet}$OTyr)(OCH_2R)] complex, (*ii*) intra-molecular H-transfer (the rate determining step) to generate a ketyl anion complex [Cu(II)(HOTyr)($^{\bullet}$O-CHR)], (*iii*) intramolecular oxidation of the ketyl radical anion to give [Cu(I)(HOTyr)] and the product O=CHR, and (*iv*) oxidation of [Cu(I)(HOTyr)] with molecular oxygen, O_2, to regenerate the initial tyrosinyl radical complex [Cu(II)($^{\bullet}$OTyr)] and H_2O_2. With EtOH as a substrate, the reaction $EtOH + O_2 \rightarrow MeCH{=}O + H_2O_2$ is exothermic by about −25 kcal mol^{-1}.

Many transition-metal catalysts have been developed over the last decades, which are capable of converting alcohols into the corresponding carbonyl compounds [9], and the combination of catalytic amounts of $(Pr_4N)^+[RuO_4]^-$ (TPAP) with *N*-methylmorpholine as oxidant proved to be very useful [10]. Especially noteworthy are catalysts derived from $Pd(OAc)_2$/pyridine (Uemura catalyst) or Pd(OAc)/phenanthroline (Sheldon catalyst), which use O_2, air, or H_2O_2 as terminal oxidants and can be even used in aqueous solutions [10–12]. Mostly the classical mechanisms frequently encountered in organometallic chemistry were proposed [12a]. A recent contribution discusses the α-hydrogen atom transfer to a coordinated tetramethyl piperdineoxide (TEMPO) radical from a copper-bonded alkoxide as the key step in alcohol oxidation [13].

With the objective to find organometallic radical complexes which are like Goase able to selectively convert primary hydroxyl functions into the corresponding aldehydes, we started to investigate rhodium and iridium aminyl radical complexes. We chose rhodium and iridium as metals because the bond energies of ligand atoms to these metals are intrinsically high and consequently the catalysts should be rather stable [14]. Aminyl radicals, $^{\bullet}NR_2$, were selected because they offer the possibility to better control the steric environment of the complex and especially to construct polydentate chelate ligands which additionally enhance the stability of the complexes. Indeed, the persistent Rh(I) aminyl radical cation [Rh($trop_2N^{\bullet}$)(bipy)]OTf **I** [15] and a neutral aminyl radical rhodium complex to which was assigned the structure [Rh($trop_2$dach-2H)]$^{\bullet}$ **II** [16] were isolated (Scheme 1).

These complexes contain chelating aminyl radicals as ligands which were constructed on the basis of the dibenzo[*a*,*d*]cyclohepten-5-yl platform (in the following we will refer to the trivial name dibenzo*trop*ylidenyl and use the abbreviation ''trop'' for this group). Pulse EPR spectroscopy in combination with DFT calculations allowed us to assign the spin distribution in both complexes. In **I**, 30% of the spin density is located at the Rh-center and 57% at the N one. In **II** we find 41% at Rh and 2 × 28% at both nitrogen centers. In accordance with these findings, both **I** and **II** abstract hydrogen from activated hydrogen donors (stannanes, R_3SnH, thiols, RSH, and in case of **II** silanes, R_3SiH)

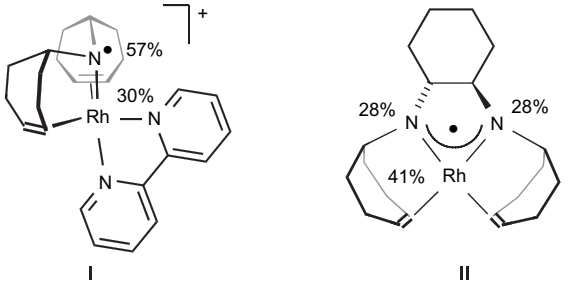

Scheme 1. Structures of rhodium aminyl radical complexes **I** and **II**.

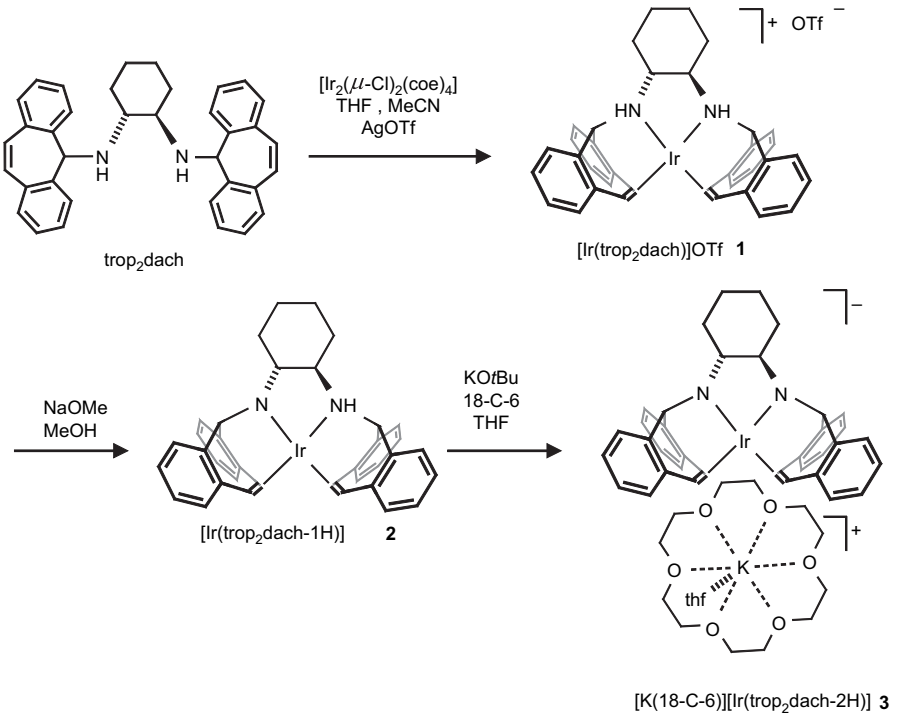

Scheme 2. Syntheses of complexes **1**–**3**.

and the corresponding amine complex [Rh(trop$_2$NH)(bipy)]OTf and amino amide [Rh(trop$_2$dach-1H)] are formed almost quantitatively. But the abstraction of α-hydrogens from alcohols was not observed. Interestingly, with the corresponding neutral iridium aminyl radical complex [Ir(trop$_2$dach-2H)]$^{\bullet}$ (**4**) and 1,4-benzoquinone (**BQ**) as hydrogen acceptor the catalytic dehydrogenation of primary alcohols to the corresponding aldehydes was observed [17].[1] This reaction proceeds with unprecedented high activity (TOFs $> 150{,}000\ h^{-1}$) even for non-activated alcohols and selectivity, that is secondary hydroxyl groups are not converted.

In this report we discuss the properties and structures of the iridium complexes [Ir(trop$_2$dach)]OTf (**1**) and [Ir(trop$_2$dach-1H)] (**2**), which are likely to be involved in the catalysis. A comparison is made with the previously reported anionic bis(amido)complex [K(18-C-6)][Ir(trop$_2$dach-2H)] (**3**) [17]. The highly efficient catalytic dehydrogenation of naturally occurring primary alcohols was investigated in order to evaluate the scope of the iridium aminyl radical-catalyzed dehydrogenation.

[1] Selected bond lengths and angles for the bis(amido)iridate [Ir(trop$_2$dach-2H)]$^-$ (average of two crystallographically independent molecules: Ir–N: 1.97025; Ir–ct 1.9985, C=C 1.44275, $\sum$(N) = 353.4°, $\varphi = 8.1°$.

2. Results

2.1. Properties of iridium trop$_2$dach complexes *1*, *2*, and *3*

The iridium complexes **1** and **2** were prepared as outlined in Scheme 2. The one-step synthesis of **3** from **1** has been reported before [17].

The neutral amino amide complex [Ir(trop$_2$dach-1H)] (**2**) is obtained from **1** by deprotonation with sodium methanolate in methanol. Under these conditions, double deprotonation to the di(amido) complex **3** is not observed. The di(amido)iridate [K(18-C-6)][Ir(trop$_2$-dach-2H)] (**3**) is obtained when **2** is treated with the stronger base KO^{t}Bu/18-crown-6 in THF. In course of the deprotonation the absorption of the longest wave length, λ_{max}, is successively red-shifted from 486 nm in **1** to 504 nm in **2** to 524 nm in **3**. We determined the pK_a values for each deprotonation step using a classical ^{1}H NMR spectroscopic technique frequently used for organic molecules [18]. For each equilibrium (1) and (2),

$$[\mathrm{Ir(trop_2dach)}]^+ + \mathrm{Ref(1)}^- \rightleftharpoons [\mathrm{Ir(trop_2dach-1H)}] + \mathrm{RefH(1)} \quad (1)$$

$$[\mathrm{Ir}(\mathrm{trop_2dach}-1\mathrm{H})] + \mathrm{Ref}^-(2) \rightleftharpoons [\mathrm{Ir}(\mathrm{trop_2dach}-2\mathrm{H})]^- + \mathrm{RefH}(2) \quad (2)$$

a suitable reference acid base pair, Ref^-/RefH, has to be found for which the pK_a is known. The first and second pK_a of **1** is then simply obtained by $\mathrm{p}K_a^1(\mathbf{1}) = \mathrm{p}K_a(\mathrm{Ref}\ 1) - K^1$ and $\mathrm{p}K_a(\mathbf{2}) = \mathrm{p}K_a(\mathrm{Ref}\ 2) - K^2$, where K^1 and K^2 are the equilibrium constants of reactions (1) and (2). The reference system should have NMR signals distinct from those of the sample system. K^1 and K^2 are determined by integration of the peak areas of selected NMR signals for each component, or, when only average signals are observed, from the relative shift of selected signals with respect to the NMR spectra of the pure acids and pure bases. It is of advantage that the reference system has a pK_a close to the one which is searched for in order to keep the experimental errors small (this is the case when all components in the equilibria (1) or (2) are in 1:1:1:1 ratio). The pK_a values of **1**, $\mathrm{p}K_a^1(\mathbf{1}) = 10.5$ and $\mathrm{p}K_a^2(\mathbf{1}) = 19.6$, were determined in [$d_6$]dimethylsulfoxide ([$d_6$]DMSO) as solvent and with the use of sodium 1,3-cyclohexandionate ($C_6H_7O_2^-$)/1,3-cyclohexandione ($C_6H_8O_2$) as reference pair (1) [$\mathrm{p}K_a^{\mathrm{DMSO}}(\mathrm{Ref}\ 1) = 10.3$] and lithium pyrrazolate/pyrrazole [$\mathrm{p}K_a^{\mathrm{DMSO}}(\mathrm{Ref}\ 2) = 19.8$] as reference pair (2). The reaction $[\mathrm{Ir}(\mathrm{trop_2dach})]^+ + C_6H_7O_2^- \rightleftharpoons [\mathrm{Ir}(\mathrm{trop_2dach\text{-}1H})] + C_6H_8O_2$ is fast on the NMR time scale, that is, averaged resonances are observed for the couples $[\mathrm{Ir}(\mathrm{trop_2dach})]^+$/$[\mathrm{Ir}(\mathrm{trop_2dach\text{-}1H})]$ and $C_6H_7O_2^-$/$C_6H_8O_2$ in the ^{1}H NMR spectrum. On the other hand, the proton-exchange reaction between $[\mathrm{Ir}(\mathrm{trop_2dach})]^+$ and $[\mathrm{Ir}(\mathrm{trop_2dach\text{-}1H})]$ is slow and sharp resonances are observed for each compound in an equimolar solution of both components.

Like the corresponding rhodium complex [Rh(trop$_2$dach)]OTf [19],[2] the iridium complex **1** is reduced in two consecutive one-electron steps, at $E^1_{1/2} = -1.87$ V to the metallo radical $[\mathrm{Ir}(\mathrm{trop_2dach})]^\bullet$ and at $E^2_{1/2} = -2.52$ V to the iridate complex $[\mathrm{Ir}(\mathrm{trop_2dach})]^-$ [all potentials vs. ferrocenium/ferrocene (Fc^+/Fc) as reference, DMSO as solvent, Pt working electrode, scan rate = 100 mV s^{-1}). No oxidation below +1 V was observed. Although we could not measure the potentials for the oxidation reactions, [Ir(trop$_2$dach-1H)] (**2**) − e → $[\mathrm{Ir}(\mathrm{trop_2dach\text{-}1H})]^{\bullet+}$ and $[\mathrm{Ir}(\mathrm{trop_2dach\text{-}2H})]^-$ (**3**) − e → $[\mathrm{Ir}(\mathrm{trop_2dach\text{-}2H})]^\bullet$, with sufficient certitude, very likely they occur at low oxidation potentials. The analogous rhodium complexes are reversibly oxidized at remarkably low potentials: [Rh(trop$_2$dach-1H)] at $E_{1/2} = -0.34$ V [19], and the di(amido) rhodate $[\mathrm{Rh}(\mathrm{trop_2dach\text{-}2H})]^-$ at $E^1_{1/2} = -1.02$ V to give the radical $[\mathrm{Rh}(\mathrm{trop_2dach\text{-}2H})]^\bullet$, which is again reversibly oxidized in a second step still at a low potential, $E_{1/2} = -0.38$ V [16,20].

Crystals suitable for X-ray diffraction of (*R*,*R*)-[Ir(trop$_2$dach)]OTf **1** were obtained from a concentrated THF solution layered with *n*-hexane and contain two THF molecules in the crystal lattice. Crystals of (*S*,*S*)-[Ir(trop$_2$dach-1H)] (**2**) with the chiral space group $P2_12_12_1$ were grown from a concentrated diethylether solution layered with *n*-pentane. They stem from one experiment where we used the racemic mixture of the trop$_2$dach ligand; that is the crystals exist in two enantiomorphic forms. In all other experiments, the enantiomerically pure (*R*,*R*)-trop$_2$dach was employed as ligand. Plots of the structures of **1** and **2** are shown in Figs. 1 and 2, selected bond lengths and angles are given in the figure captions and pertinent crystal data are given in Table 1 in the experimental section. In **1** and **2**, the iridium center is embedded in a tetrahedrally distorted planar coordination sphere as is indicated by the angle φ given by the intersection of the N1–Ir–ct1 and N2–Ir–ct2 plane, which amounts to 20°. There is remarkable little change of the bond lengths and angles when **1** is deprotonated to **2**. One would expect that the amide nitrogen center, N1 in **2**, exerts a trans-influence leading to a lengthening of the distances to

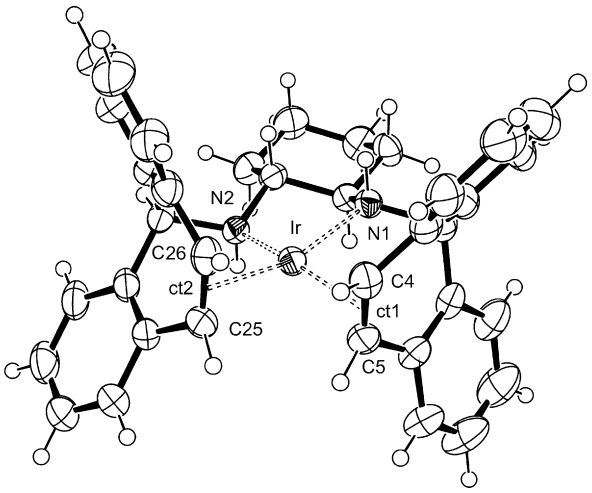

Fig. 1. Plot of the structure of the cation in (*R*,*R*)-[Ir(trop$_2$dach)]Otf (**1**). The disordered triflate anion and THF molecules are omitted for clarity. Selected bond lengths [Å] and angles [°]: Ir–N1 2.095(3), Ir–N2 2.090(3), Ir–ct1 1.986(4), Ir–ct2 2.004(4), C4–C5 1.421(6), C25–C26 1.401(6); ∑(N1) 339.6, ∑(N2) 340.9. The angle φ, defined by intersection of the N1–Ir–ct1 and the N2–Ir–ct2 plane, amounts to 20.6°.

[2] [Rh(I)(trop$_2$dach)]+/[Rh(0)(trop$_2$dach)]: $E^1_{1/2} = -1.83$ V; [Rh(0)(trop$_2$dach)]/[Rh(−I)(trop$_2$diamine)]$^-$: $E^2_{1/2} = -2.27$ V.

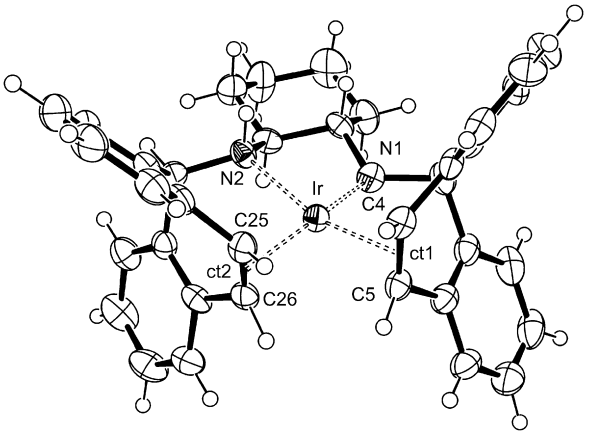

Fig. 2. Plot of the structure of (*S*,*S*)-[Ir(trop$_2$dach-1H)] (**2**). The pentane molecule, incorporated in the unit cell, is omitted for clarity. Selected bond lengths [Å] and angles [°]: Ir–N1 1.995(5), Ir–N2 2.143(5), Ir–ct1 2.026(6), Ir–ct2 2.026(6), C4–C5 1.448(9), C25–C26 1.468(9); ∑(N1) 353.0, ∑(N2) 338.7. The angle φ, defined by intersection of the N1–Ir–ct1 and the N2–Ir–ct2 plane, amounts to 20.1°.

the opposite ligands [21,22]. This is not the case. The distances between the iridium atom and the centroids, ct, of the coordinated C=C$_{trop}$ groups remain almost constant, at about 2.0 Å. Obviously, the C=C$_{trop}$ units serve as a kind of ''electronic buffer'' and absorb the electron density donated by the amide groups by efficient metal-to-ligand back-donation [that is the increased electron population in the filled d-orbitals at the iridium center is depleted by donation into the π* orbitals of the coordinated C=C$_{trop}$ groups, d(Ir) → π*(C=C$_{trop}$)].

In line with this interpretation, the coordinated C=C bond trans to the amide nitrogen N1 is slightly lengthened in **2**. The Ir–N bonds become slightly shorter upon deprotonation and shrink below a length of 2.0 Å while the Ir–amine bonds, Ir–NH, are slightly longer than 2.0 Å. Note that the sum of the C–N–C and two Ir–N–C bond angles, ∑(N), becomes significantly larger by about 13° when the NH function is deprotonated, but the amide nitrogen still has a slightly pyramidal coordination sphere [∑(N1) = 353.0°]. The discussed structural trends hold also for the diamido complex [Ir(trop$_2$dach-2H)]$^-$, that is the Ir–N bonds are <2.0 Å, the coordinated C=C$_{trop}$ units elongated, and ∑(N1) ≈ 353°. Only the complex adopts a lesser distorted structure closer to a planar one (φ = 8.1°).

In Table 2, the ^{1}H NMR and ^{13}C NMR data of the olefinic protons and carbon nuclei of the coordinated C=C$_{trop}$ groups of **1** and **2** are given. The last column shows the chemical shifts of the NH protons of the coordinated amine functions. For comparison we list also the corresponding data for the diamidoiridate **3** and the rhodium complexes [Rh(trop$_2$dach)]$^+$, [Rh(trop$_2$dach-1H)], and the anion [Rh(trop$_2$dach-2H)]$^-$.

Table 1
Crystal data and refinement of compounds **1**, **2**, and **3**

Compound	**1**	**2**	**3**
Empirical formula	$C_{45}H_{50}F_3IrN_2O_2S$	$C_{41}H_{45}IrN_2$	$C_{56}H_{72}IrKN_2O_8$
M	980.13	757.99	1132.46
Crystal system	Monoclinic	Orthorhombic	Monoclinic
Space group	$P2_1$	$P2_12_12_1$	$P2_1$
a/Å	9.3769(6)	13.075(2)	11.7856(7)
b/Å	17.870(1)	15.655(3)	24.750(1)
c/Å	12.6318(8)	17.739(3)	17.254(1)
α/°			
β/°	103.627(1)		95.342(1)
γ/°			
V/Å^3	2057.1(2)	3631(1)	5010.9(5)
μ/mm^{-1}	3.358	3.706	2.805
D_{calcd}/g cm^{-3}	1.582	1.387	1.501
Crystal dimensions/mm	0.23 × 0.20 × 0.18	0.17 × 0.15 × 0.14	0.31 × 0.23 × 0.21
Z	2	4	4
T/K	298	200	200
$2\theta_{max}$/°	56.64	55.26	56.58
Refls. measured	21,460	20,454	69,595
Refls. unique	10197 (R_{int} = 0.0216)	7665 (R_{int} = 0.0608)	24616 (R_{int} = 0.0304)
Parameters/restraints	587/33	397/38	1225/14
*R*1 [$I \geq 2\sigma(I)$]	0.0267	0.0376	0.0302
*wR*2 (all data)	0.0636	0.0895	0.0685
Max./min. res. elec. dens./e Å^{-3}	1.089/−0.399	1.499/−1.375	1.611/−0.502

Table 2
^{1}H and ^{13}C NMR resonances [ppm] of the C*H*=C*H*$_{trop}$ units and the NH function in **1**, **2**, and **3**

	$\delta\ ^{1}H_{ol}$	$\delta\ ^{1}H_{ol}$	$\delta\ ^{13}C_{ol}$	$\delta\ ^{13}C_{ol}$	$\delta\ ^{1}H(N)$
[Ir(trop$_2$dach)]$^+$ (**1**)	4.02	4.75	60.4	67.5	5.92
[Ir(trop$_2$dach-1H)] (**2**)	2.66[a]	3.34[a]	47.8[a]	51.4[a]	–
	3.46	4.09	54.8	62.9	5.74
[Ir(trop$_2$dach-2H)]$^-$ (**3**)	2.63	2.91	49.8	52.5	–
[Rh(trop$_2$dach)]$^+$	4.16	5.38	70.1	83.4	4.45
[Rh(trop$_2$dach-1H)]	2.99[a]	3.49[a]	67.0[a]	67.3[a]	–
	4.29	4.83	71.2	81.4	5.07
[Rh(trop$_2$dach-2H)]$^-$	2.90	3.79	66.4	73.0	–

[a] Data for C=C$_{trop}$ unit trans to the amide nitrogen N1.

The data are fully in accord with the structures determined in the crystalline state. Due to the tetrahedral distortion and the chirality of the ligand backbone leading to C_2-symmetric structures for **1** and **3**, the $^{1}H_{ol}$ and $^{13}C_{ol}$ resonances become pairwise inequivalent and two resonances are observed. The neutral amine amide complexes [M(trop$_2$dach-1H)] are asymmetric and consequently four distinct signals are obtained. Upon deprotonation, both the $^{1}H_{ol}$ and $^{13}C_{ol}$ resonances of the C=C$_{trop}$ bond opposite to the amide group are considerably shifted toward lower frequencies (that is more shielded than the C=C$_{trop}$ units, opposite to the NH amine functions). This finding bolsters the above-made statement that the C=C$_{trop}$ bonds function as electronic buffers and accept the increasing electron density at the metal centers in the deprotonated species. Note that generally the $^{1}H_{ol}$ and $^{13}C_{ol}$ resonances are recorded at significantly lower frequencies in the iridium complexes when compared to the rhodium analogues. This strong shielding indicates that metal-to-ligand back-donation d(M) → π*(C=C$_{trop}$) is more effective in the iridium complexes. Consequently, the filled d-orbitals at the metal are polarized towards the C=C$_{trop}$ units and away from the occupied p-type orbitals at the amide nitrogen centers representing the amide lone-pairs. The destabilizing 2-center-4-electron d(M)–p(N) interaction is diminished. Hence, the amido complexes **2** and **3** become less destabilized when compared to their rhodium counterparts and consequently the acids conjugated with **2** and **3**, namely the amine complexes **1** and **2**, become more acidic. Indeed, [Ir(trop$_2$dach)]$^+$ (**1**) is five order of magnitude more acidic than [Rh(trop$_2$dach)]$^+$ and the NH function in [Ir(trop$_2$dach-1H)] (**2**) is about 3–4 orders of magnitude more acidic than the one in [Rh(trop$_2$dach-1H)]. This is also clearly reflected by the more deshielded ^{1}H NMR shifts of the amine protons in the iridium complexes **1** and **2** (Table 2). We had previously used this argumentation based on avoided filled–filled repulsions which was introduced by Caulton [23] to qualitatively interpret the physico-chemical properties of a series of [Rh(trop$_2$dach)] complexes.

2.2. Oxidation of natural primary alcohols

Based on the mechanism for GOase, we proposed a catalytic cycle [17] which is presented in Scheme 3 in simplified form. The cationic bis(amino) complex **1** is doubly deprotonated by a base (KO^{t}Bu) to give the anionic bis(amido) complex **3**, which is subsequently oxidized by 1,4-benzoquinone (**BQ**) to the iridium aminyl radical complex **4** and the semiquinone radical anion (**SQ**$^{\bullet-}$). Both **4** and **SQ**$^{\bullet-}$ were detected by EPR spectroscopy [17]. As with GOAse, it is possible that the alcohol RCH$_2$OH (or more likely the corresponding alkoxide) is coordinated to the iridium center whereby the α-hydrogen is placed in proximity to the nitrogen centered radical. Intra-molecular H-atom transfer may occur and an Ir-coordinated ketyl radical anion is formed. Likely this is oxidized in an inter-molecular reaction by **SQ**$^{\bullet-}$ to give the product, RCH=O, and catechol (**Cat**). It was found that a wide range of simple aliphatic alcohols, arenes and heterocyclic compounds with primary hydroxyl functions can be converted to the corresponding aldehydes.

We tested now some more complex naturally occurring alcohols as substrates in the catalytic dehydrogenation reaction. The reactions with geraniol (**5**), retinol (**6**) and (±)-lavandulol (**7**) were performed at 100 °C in chlorobenzene, which had proven to be a suitable solvent [17]. At a substrate-to-catalyst ratio S/C = 10,000 (0.01 mol% catalyst loading), complete and clean conversion of **5** and **6** to geranial **8** and retinal **9**, respectively, were observed within minutes (Tables 3 and 4). The sterically more congested alcohol (±)-lavandulol **7** was much slower converted. At S/C = 10,000, not more than 30% of the alcohol was consumed, even after longer reaction times.

Therefore the S/C ratio was lowered to 1000 and under these conditions, comparable higher conversions were observed. However, we observed the formation of the isomerized product isolavandulal **11** beside (±)-lavandulal **10**, which is clearly indicated by the singlet resonance of the aldehyde proton, C*H*=O, at $\delta = 10.1$ ppm beside the doublet at $\delta = 9.5$ ppm, typical of the C*H*=O of (±)-lavandulal **10**. Isolavandulal **11** was isolated from the reaction mixture, purified and identified by comparison with the ^{1}H NMR data reported in the literature [24,25].

To study the parameters that influence the formation of (±)-lavandulal **10** and isolavandulal **11**, the catalytic

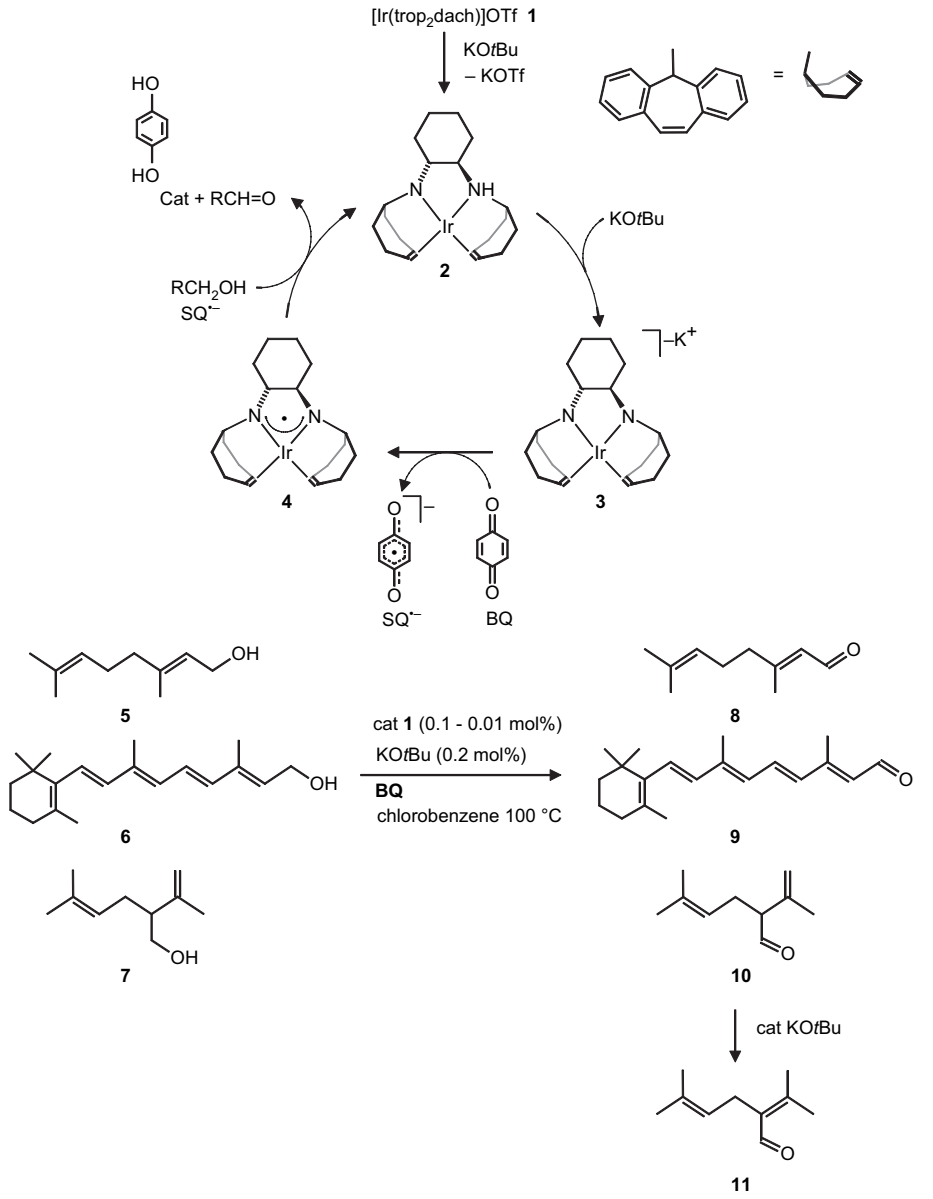

Scheme 3. Proposed catalytic cycle for the conversion of the natural alcohols geraniol (**5**), retinol (**6**) and (±)-lavandulol (**7**).

Table 3
Catalytic dehydrogenation of geraniol (**5**), retinol (**6**) and (±)-lavandulol (**7**)

Substrate	Product(s)	Yield	Time
Geraniol **5**	Geranial **8**	>98%	20 min
Retinol **6**	Retinal **9**	>98%	5 min
(±)-Lavandulol **7**	(±)-Lavandulal **10**	cf Table 4	
	Isolavandulal **11**		

Conditions: chlorobenzene, 100 °C, 0.01 mol% catalyst loading, 0.22 mol% KO^{t}Bu, 1.33 equiv 1,4-benzoquinone vs. substrate.

oxidation of (±)-lavandulol was performed under varying conditions: 0.1 mol% (entries 1–3) and 0.02 mol% (entry 4) of the catalyst precursor **1** were used, the catalytic amount of KO^{t}Bu was varied between 0.22 and 0.66 mol%, and the amount of **BQ** was varied from 1.33 to 2.66 equivalents with respect to lavandulol **7**.

Clearly, the amount of isolavandulal **11** increases with increasing base concentration (compare entries 1 and 2) and with increasing reaction times (entry 4). With smaller amounts of base and larger concentrations of **BQ**, about 90% of total conversion to aldehydes **10** and **11** is obtained and (±)-lavandulal **10** can be

Table 4
Dehydrogenation of (±)-lavandulol **7** under various conditions

	S/C ratio	KO^{t}Bu[a] (equiv)	**BQ**[b] (equiv)	Time (h)	Yield (%)	Ratio **10**:**11**
1	1000	22	1.33	21	76	68:32
2	1000	66	1.33	19	57	0:100
3	1000	22	2.66	4	90	94:6
4	5000	44	2.66	168	57	7:93

[a] Equivalents of base with respect to catalyst.
[b] Equivalents of **BQ** with respect to substrate.

obtained as the main product (entry 3). On the other hand, with low catalyst loadings, longer reactions times, and relatively high base concentration, the main product is isolavandulal **11** (entry 4).

The evolution of the ratio of **10**:**11** was followed with time under otherwise identical conditions (0.1 mol% catalyst, 66 equiv KO^{t}Bu, 1.33 equiv **BQ**). The result is displayed in Fig. 3, which clearly shows that the total conversion to aldehydes **10** and **11** does not significantly change while increasing amounts of isolavandulal **11** are formed. The experiments thus strongly indicate that the isomerization **10** to **11** is a classical base-catalyzed reaction and is not influenced by the metal complex.

3. Conclusion

In conclusion, it was shown that the iridium trop$_2$dach complexes have very similar ground-state structures compared to their rhodium counterparts. Remarkably, the iridium complexes are significantly more acidic, which can be explained by a stronger metal-to-olefin back-donation, which especially stabilizes the amido complexes. These are relatively easily oxidized and a metallo radical like [Ir(trop$_2$dach-2H)]$^{\bullet}$ **4** is very likely involved in the very efficient catalytic conversion of natural primary alcohols like geraniol and retinol to the corresponding aldehydes, geranial and retinal. Sterically more congested alcohols are converted at lower rates. This suggests that the exclusive conversion of primary alcohols to aldehydes has primarily steric reasons. We believe that our observation that metal-coordinated radicals can be used for highly *efficient and selective* reactions is an important metalloenzyme-inspired finding, which may lead to the development of new types of catalysts.

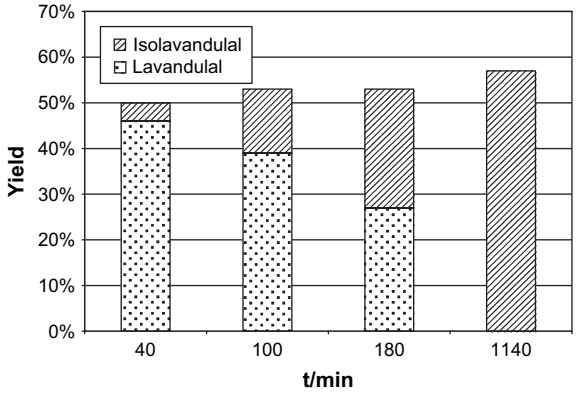

Fig. 3. Time-dependent isomerization of (±)-lavandulal **10** to isolavandulal **11** after dehydrogenation of (±)-lavandulol **7**. Reaction conditions: catalyst loading 0.1 mol%, 0.66 mol% KO^{t}Bu, 1.33 equiv **BQ** with respect to **7**.

4. Experimental part

4.1. General procedure

All manipulations of air or moisture sensitive compounds were performed on a standard vacuum line in flame-dried glassware under an atmosphere of argon (purified with an MBraun 100 HP gas purification system). Solvents were distilled under argon from sodium/benzophenone (THF, hexane), calcium hydride (acetonitrile), and phosphorus pentoxide (chlorobenzene). Air-sensitive compounds were stored and weighed in a glove-box (M Braun: Labmaster 130 or 150B-G). Reactions performed with small quantities of compound were performed in a glove-box.

NMR measurements were carried out on Bruker Avance 200, 250 and 300 MHz spectrometers at room temperature. Chemical shifts δ are given by definition as dimensionless numbers. The absolute values of the coupling constants are given in hertz (Hz), regardless of their signs. The assignments were accomplished using multi-dimensional methods. Multiplicities are abbreviated as singlet (s), doublet (d), triplet (t), quartet (q), and broad (br). Spectra were referenced with external standards: for ^{1}H and ^{13}C NMR with TMS and for ^{19}F NMR with $CFCl_3$.

UV/vis spectra were recorded on a UV/vis/NIR lambda 19 spectrometer in 5-mm quartz cuvettes (200–1000 nm).

Gas chromatography was performed on a Hewlett Packard HP 6890 Series GC system equipped with a HP-5 crosslinked 5% PH ME siloxane column (30 m × 0.32 mm, film thickness 0.25 μm), flow rate 27.2 mL/min at 1.42 psi. The following temperature program was used: initial temperature 80 °C (hold 1 min), increase to 180 °C at a rate of 4 °C/min and hold for 40 min.

Cyclic voltammetric investigations were performed using a Princeton Applied Research potentiostat/

galvanostat model 263A. Working electrode: planar platinum electrode (approximate surface area 0.785 mm^2); reference electrode: silver; counter electrode: platinum wire. A 0.1 M solution of nBu$_4$NPF$_6$ in dimethylsulfoxide (DMSO) was used as electrolyte. A scan rate of 100 mV s^{-1} was used and at the completion of each measurement, ferrocene (Fc) was added as an internal standard for calibration.

(*R*,*R*)-[Ir(trop$_2$dach)]OTf (**1**): 300 mg [Ir$_2$(μ-Cl)$_2$(coe)$_4$] (0.34 mmol) are dissolved in 25 mL THF and 331 mg (0.68 mmol) trop$_2$dach and a few drops of CH_3CN are added. To this red solution 172 mg (0.68 mmol) of silver triflate is added and a white solid precipitates. After stirring for 1 h at r.t., the reaction mixture is filtered through Celite. All volatiles are removed in vacuo and the raw product is crystallized from THF/hexane (1:1), yielding 259 mg (309 mmol, 91%) of the product as red crystals. After decanting the solvent, the product is thoroughly dried in vacuo. For ^{1}H NMR and ^{13}C NMR data of diagnostic value, see Table 2. – ^{19}F NMR (188.3 MHz, d_8-THF): $\delta = -80.7$ (s, OTf). UV/vis (THF): λ [nm]: 486, 397, 306.

(*R*,*R*)-[Ir(trop$_2$dach)-1H] (**2**): To a solution of 180 mg of **1** (0.22 mmol) in methanol, sodium methanolate is added. The color changes to dark red and all volatiles are removed in vacuo. The raw product is dissolved in diethyl ether and stirred for 20 min. After filtering, the precipitate of the solution is layered with hexane and red crystals grow overnight to yield 129 mg (0.19 mmol, 86%) of the product. For ^{1}H NMR and ^{13}C NMR data of diagnostic value, see Table 2. – UV/vis (THF): λ [nm]: 504, 423, 280.

(*R*,*R*)-[K(18-C-6)][Ir(trop$_2$dach)-2H] (**3**): To a solution of 100 mg of **1** (0.12 mmol) in THF, 29 mg KO^{t}Bu (0.26 mmol) and 32 mg 18-C-6 (0.12 mmol) are added. The color changes to dark red and the solution is layered with hexane. Red crystals grow overnight to yield a dark red powder, 101 mg (0.11 mmol, 94%). For ^{1}H NMR and ^{13}C NMR data of diagnostic value, see Table 2. – UV/vis (THF): λ [nm]: 524, 355, 274.

Catalyses: The catalyst precursor was dissolved under stirring in chlorobenzene; reactions with a S/C ratio of 10,000 and 5000 were conducted in 25 mL solvent, 1000 in 6 mL solvent. First, KO^{t}Bu and then after 5 min alcohol was added. The mixture was heated to 100 °C and **BQ** was added in one portion. The reactions were then monitored by GC and ^{1}H NMR.

4.2. Work-up procedure for lavandulyl aldehydes

The reaction mixture was filtered through Celite and the solvent removed in vacuo (45 °C, 40 mbar). ^{1}H NMR spectra showed, according to the progression of the reaction, a mixture of the alcohol and the respective aldehyde(s). To further purify isolavandulal **11**, the dark, oily residues were filtered through aluminum oxide and washed with chlorobenzene. Again, the solvent was removed in vacuo. The aldehyde **11** was then obtained as an oil, contaminated with traces of quinones and therefore still rather dark in color. ^{1}H NMR data of **11** were found to be in agreement with the literature [19,20].

4.3. X-ray diffraction studies: details of the data collection and refinement for *1*, *2*, and *3*

Crystals suitable for X-ray analysis were mounted in degassed perfluoropolyalkylether on top of a glass fiber and then brought into the cold nitrogen stream of a low temperature device so that the oil solidified. Data collection for the X-ray structure determinations were performed on Bruker SMART Apex diffractometer system with CCD area detector by using graphite-monochromated Mo Kα (0.71073 Å) radiation and a low-temperature device. All calculations were performed using the SHELXTL (ver. 6.12) and SHELXL-97. The structures were solved by direct methods and successive interpretation of the difference Fourier map, followed by full-matrix least-squares refinement (against F^2). Moreover, an empirical absorption correction using SADABS (ver. 2.03) was applied to all structures. All non-hydrogen atoms were refined anisotropically and the contribution of the hydrogen atoms, in their calculated positions, was included in the refinement using a riding model. The residual electron densities were located close to the heavy atom iridium in all structures, even when an absorption correction was applied. The thf molecules, (**1**) and (**3**), and the pentane molecule (**2**) in the crystal lattice are slightly disordered and a high number of restraints are used to achieve a satisfactory *wR*2 value. Crystallographic data (excluding structure factors) for the structures reported in this paper have been deposited with the Cambridge Crystallographic Data Centre as supplementary publication No. CCDC-622198 (**1**), CCDC-622199 (**2**) and CCDC-622200 (**3**). Copies of the data can be obtained free of charge on application to CCDC, 12 Union Road, Cambridge CB2 1EZ, UK (fax: (+44) 1223-336-033; e-mail: deposit@ccdc.cam.ac.uk).

References

[1] J.W. Whittaker, Arch. Biochem. Biophys. 433 (2005) 227.
[2] P. Chaudhuri, K. Wieghardt, T. Weyhermüller, T.K. Paine, S. Mukherjee, C. Mukherjee, Biol. Chem. 386 (2005) 1023.

[3] J.-L. Pierre, F. Thomas, C. R. Chimie 8 (2005) 65.
[4] R.C. Pratt, T.D.P. Stack, Inorg. Chem. 44 (2005) 2367.
[5] P. Gamez, I.A. Koval, J. Reedijk, Dalton Trans. (2004) 4079.
[6] B.A. Jazdewski, W.B. Tolman, Coord. Chem. Rev. 200–202 (2000) 633.
[7] I.E. Markó, P.R. Giles, M. Tsukazaki, S.M. Brown, C.J. Urch, Science 274 (1996) 2044.
[8] L. Guidoni, K. Spiegel, M. Zumstein, U. Röthlisberger, Angew. Chem., Int. Ed. Engl. 43 (2004) 3286.
[9] There is a vast body of literature on this topic. For a recent publication giving a comprehensive listing: M.J. Schultz, S. Hamilton, D.R. Jensen, M.S. Sigman J. Org. Chem. 70 (2005) 3343.
[10] S.V. Ley, J. Norman, W.P. Griffith, S.P. Marsden, Synthesis (1994) 639.
[11] G.-J. ten Brink, I.W.C.E. Arends, R.A. Sheldon, Science 287 (2000) 1636.
[12] Reviews:(a) R.A. Sheldon, I.W.C.E. Arends, A. Dijksman, Catal. Today 57 (2000) 157;
(b) R.A. Sheldon, I.W.C.E. Arends, G.-J. Ten Brink, A. Dijksman, Acc. Chem. Res. 35 (2002) 774;
(c) R. Irie, T. Katsuki, Chem. Rec. 4 (2004) 96;
(d) S.S. Stahl, Angew. Chem., Int. Ed. Engl. 43 (2004) 3400;
(e) T. Nishimura, S. Uemura, Synlett (2004) 201.
[13] P. Gamez, I.W.C.E. Arends, R.A. Sheldon, J. Reedijk, Adv. Synth. Catal. 346 (2004) 805.
[14] T. Marks, Bonding Energetics in Organometallic Compounds, 428, ACS Symposium Series, 1990.
[15] T. Büttner, J. Geier, G. Frison, J. Harmer, C. Calle, A. Schweiger, H. Grützmacher, Science 307 (2005) 235.
[16] P. Maire, M. Königsmann, A. Sreekanth, J. Harmer, A. Schweiger, H. Grützmacher, J. Am. Chem. Soc. 128 (2006) 6578.
[17] M. Königsmann, N. Donati, J. Harmer, A. Sreekanth, H. Grützmacher, Angew. Chem. Int. Ed. Engl. 46 (2007).
[18] F.G. Bordwell, Acc. Chem. Res. 21 (1988) 456.
[19] P. Maire, F. Breher, H. Schönberg, H. Grützmacher, Organometallics 24 (2005) 3207.
[20] P. Maire, F. Breher, H. Grützmacher, Angew. Chem., Int. Ed. 44 (2005) 6325.
[21] P. Maire, T. Büttner, F. Breher, P. Le Floch, H. Grützmacher, Angew. Chem. 117 (2005) 6477;
Angew. Chem., Int. Ed. 44 (2005) 6318.
[22] T. Büttner, F. Breher, H. Grützmacher, Chem. Commun. (2004) 2820.
[23] K.G. Caulton, New J. Chem. 18 (1994) 25.
[24] J.-P. Wolf, H. Pfander, Helv. Chim. Acta 69 (1986) 62.
[25] J. Celebuski, M. Rosenblum, Tetrahedron 41 (1985) 5741.